J Neurophysiol 96: 2307–2318, 2006.
First published July 12, 2006; doi:10.1152/jn.00149.2006.

Synaptic Democracy in Active Dendrites

Clifton C. Rumsey[1] and L. F. Abbott[2]

[1]*Center for Learning and Memory, The University of Texas at Austin, Austin, Texas; and* [2]*Center for Neurobiology and Behavior, Department of Physiology and Cellular Biophysics, Columbia University College of Physicians and Surgeons, New York, New York*

Submitted 13 February 2006; accepted in final form 4 July 2006

Rumsey, Clifton C. and L. F. Abbott. Synaptic democracy in active dendrites. *J Neurophysiol* 96: 2307–2318, 2006. First published July 12, 2006; doi:10.1152/jn.00149.2006. Given the extensive attenuation that can occur along dendritic cables, location within the dendritic tree might appear to be a dominant factor in determining the impact of a synapse on the postsynaptic response. By this reasoning, distal synapses should have a smaller effect than proximal ones. However, experimental evidence from several types of neurons, such as CA1 pyramidal cells, indicates that a compensatory strengthening of synapses counteracts the effect of location on synaptic efficacy. A form of spike-timing-dependent plasticity (STDP), called anti-STDP, combined with non-Hebbian activity-dependent plasticity can account for the equalization of synaptic efficacies. This result, obtained originally in models with unbranched passive cables, also arises in multicompartment models with branched and active dendrites that feature backpropagating action potentials, including models with CA1 pyramidal morphologies. Additionally, when dendrites support the local generation of action potentials, anti-STDP prevents runaway dendritic spiking and locally balances the numbers of dendritic and backpropagating action potentials. Thus in multiple ways, anti-STDP eliminates the location dependence of synapses and allows Hebbian plasticity to operate in a more "democratic" manner.

INTRODUCTION

The phrase "dendritic democracy" has been used to describe an equalization of synaptic efficacies so that all synapses of a neuron have the same potential for affecting the postsynaptic response regardless of their locations along the dendritic tree (Häusser 2001). To compensate for dendritic attenuation, the conductance of a distal synapse must be greater than that of a more proximal one if both are to be equally effective at inducing axonal action potentials. Several types of neurons exhibit distance-dependent synaptic conductances of this form (reviewed in Häusser and Mel 2003; Williams and Stuart 2003). Examples include CA1 pyramidal neurons (Andersen et al. 1980; Andrásfalvy and Magee 2001; Andrásfalvy et al. 2003; Magee and Cook 2000; Pettit and Augustine 2000; Smith et al. 2003; Stricker et al. 1996), CA1 stratum radiatum interneurons (Pettit and Augustine 2000), spinal motoneurons (Alvarez et al. 1997; Iansek and Redman 1973; Jack et al. 1981; Pierce and Mendell 1993), spinal Ia inhibitory interneurons (Alvarez et al. 1997), and goldfish Mauthner cells (Korn et al. 1993; Sur et al. 1995; Triller et al. 1990). In CA1 pyramidal neurons, synaptic equalization is correlated with an increase in the number of AMPA receptors at more distal synapses (Andrásfalvy and Magee 2001; Magee and Cook 2000; Smith et al. 2003). Distance-dependent synaptic strengths are not seen in neocortical layer V pyramidal neurons (Williams and Stuart 2002), but other experiments suggest that location-dependent differences in glutamate receptor distribution may occur in at least some cortical layer V pyramidal cells (Dodt et al. 1998; Frick et al. 2001).

Evidence for equalization of synaptic efficacy raises questions about the mechanisms that allow synapses to determine their position with respect to the soma/axon and modify their strengths to compensate for the resulting attenuation (Rabinowitch and Segev 2006). In a previous paper (Rumsey and Abbott 2004a), we argued that the answer might lie in a particular form of spike-timing-dependent plasticity (STDP) called anti-STDP. In what we will call STDP (without the anti-), a presynaptic action potential followed by a postsynaptic spike within a temporal window on the order of tens of milliseconds generates long-term potentiation (LTP), and post-before-presynaptic spiking generates long-term depression (LTD). STDP (reviewed in Bi and Rubin 2005) has been studied extensively both experimentally (Bi and Poo 1998; Debanne et al. 1998; Feldman 2000; Froemke and Dan 2002; Froemke et al. 2005; Markram et al. 1997; Sjöström et al. 2001, 2003; Zhang et al. 1998) and theoretically (Gütig et al. 2003; Kempter et al. 2001; Kistler and van Hemmen 2000; Roberts 2000; Roberts and Bell 2000; Rubin 2001; Rubin et al. 2001; Senn et al. 2001; Song and Abbott 2001; Song et al. 2000; van Rossum et al. 2000; Williams et al. 2003).

Anti-STDP is so-named because its timing dependence is the opposite of STDP. In other words, generally speaking, pre-before-postsynaptic spiking induces LTD and post-before-presynaptic spiking induces LTP. Particular forms of anti-STDP have been observed in cells in the electrosensory system of a weakly electric fish (Bell et al. 1997; Han et al. 2000), the cerebellum (Wang et al. 2000), and the dorsal cochlear nucleus of the brain stem (Tzounopoulos et al. 2004). Anti-STDP has also been investigated theoretically (Roberts 2000; Roberts and Bell 2000, 2002; Rumsey and Abbott 2004a,b; Williams et al. 2003). Anti-STDP is particularly suited to function as a mechanism for equalizing synaptic efficacies where efficacy refers to the likelihood of a presynaptic action potential evoking a postsynaptic spike. Because STDP differentiates between presynaptic spikes that precede and thus contribute to postsynaptic spiking and those that do not, STDP and anti-STDP are sensitive to synaptic efficacy. STDP uses this sensitivity to potentiate the synapses most effective at generating postsynaptic action potentials and to weaken less effective ones. Anti-STDP, on the other hand, equalizes efficacies.

Previously, we investigated equalization by anti-STDP in unbranched, passive cable models (Rumsey and Abbott

Address for reprint requests and other correspondence: C. C. Rumsey, The University of Texas at Austin, Center for Learning and Memory, 1 University Station C7000, Austin, TX 78712 (E-mail: rumsey@mail.clm.utexas.edu).

The costs of publication of this article were defrayed in part by the payment of page charges. The article must therefore be hereby marked "*advertisement*" in accordance with 18 U.S.C. Section 1734 solely to indicate this fact.

2004a,b). In a passive cable with a relatively low total synaptic conductance, anti-STDP equalizes both the synaptic efficacies and the amplitudes of somatic excitatory postsynaptic potentials (EPSPs) for synapses distributed across the length of the cable. In a model with a higher total synaptic conductance, which effectively increases the electrotonic length of the cable, anti-STDP still equalizes synaptic efficacies, but the equalization of somatic EPSPs extends only partway along the cable (Rumsey and Abbott 2004a). We now extend this work to active and branched cables. This extension not only allows us to investigate more complex models and reveal new features of anti-STDP, it also allows us to correct for a simplification made previously. Our earlier results relied on the assumption that every synapse is informed automatically whenever an action potential is generated at the soma. In reality, this information is only conveyed to synapses by means of backpropagating action potentials (Häusser et al. 2000; Stuart and Sakmann 1994; Stuart et al. 1997a,b). A number of issues arise because of this, including whether failures or delays of backpropagation prevent anti-STDP from equalizing synaptic efficacies. Our current models include active dendritic conductances that support backpropagating action potentials (bAPs), allowing us to address these and other issues.

Equalizing synaptic efficacies along a long passive dendritic cable may require potentiating the most distal synapses to unrealistic degrees. In this situation, a local spike-generation zone in the distal dendrite can boost the efficacy of distal synapses, allowing distal efficacies to be equalized with proximal efficacies by anti-STDP without requiring unrealistic synaptic potentiation (Rumsey and Abbott 2004b). Finally, equalization of synaptic efficacies is an important prelude to applying any form of Hebbian plasticity, such as STDP, to synapses. If this is not done, the advantage that proximal synapses have over distal synapses in controlling firing will cause them to be potentiated preferentially at the expense of distal synapses (Rumsey and Abbott 2004a,b). In active dendrites, this can generate dendritic regions that dominant activity at the expense of other branches that become functionally silent (Goldberg et al. 2002). Models that include active branched dendrites allow us to address all of these issues.

Biophysically based models of STDP have been developed (Abarbanel et al. 2003; Castellani et al. 2005; Rubin et al. 2005), but we do not make use of these here. One reason for this is that we are employing anti-STDP not STDP, and it is not clear how to modify these models so that they apply to anti-STDP. In addition, use of a biophysical model would require us to duplicate the calcium dynamics in dendritic spines with great accuracy, something that has been attempted (Franks and Sejnowski 2002) but is beyond the scope of the modeling we do here. Although our models are anatomically detailed, they are cruder when it comes to the less-known details of active dendritic conductances. Our purpose is not to present an exhaustive model of dendritic initiation or backpropagation of action potentials. Instead, we want to examine how dendritic structure and the propagation delays it implies and how independent dendritic and somatic spike initiation affect the equalization of synaptic efficacies. Our models are constructed with these goals in mind.

METHODS

We studied the effects of anti-STDP in multi-compartmental models with two different morphologies. One morphology was a single unbranched, cylindrical cable that acted as an equivalent cable for a full dendritic tree. The other was based on a reconstruction of a CA1 pyramidal cell. All simulations were done using the program NEURON (Hines and Carnevale 1997). The integration time step in the simulations was 0.1 ms. Smaller time steps were also investigated and do not alter the results.

Cylindrical cable model

The cylindrical cable model consisted of a somatic compartment connected to a single, 50-compartment, unbranched cable acting as an equivalent cable for an extended dendritic tree. The cylindrical somatic section had a diameter of 20 μm and a length of 20 μm, and the dendritic cable had a diameter of 2 μm and a length of 1,000 μm. The resting potential of the soma was -69.8 mV. The membrane capacitance of both soma and dendrite was 1 μF/cm^2. The cable had an axial resistivity of 50 Ω-cm. Both the soma and dendrite had a leakage conductance of 5×10^{-5} S/cm^2, and the leakage reversal potential was -60 mV in the soma and -55 mV in the dendrite. Postsynaptic action potentials were generated at the somatic compartment by the standard Hodgkin-Huxley sodium and potassium conductances included in the NEURON program (Hines and Carnevale 1997). The maximum sodium channel conductance in the soma was set to 0.38 S/cm^2. The dendritic cable contained the same Hodgkin-Huxley conductances, and the maximum sodium conductance was set to increase linearly from 0.01 S/cm^2 at the proximal end to 0.06 S/cm^2 at the distal end. One hundred excitatory synapses were placed uniformly along the cable, two of them per cable compartment, and 20 inhibitory synapses were also placed uniformly along the cable.

CA1 pyramidal morphology models

The models with full neuron morphology were based on a reconstructed CA1 pyramidal neuron. The cell was *n123* from the Duke/Southampton Archive of Neuronal Morphology (http://neuron.duke.edu/cells/index/topindex.html) (cell published in Pyapali et al. 1998). The membrane conductances included in the model were a passive leak conductance, a fast sodium conductance, and a persistent voltage-dependent potassium conductance. The sodium and potassium conductances had Hodgkin-Huxley kinetics as described in Mainen et al. (1995). All details are as given in that reference with the exception that the sodium inactivation $V_{1/2}$ for h_∞ was modified from -65 to -50 mV to compensate for the fact that our model received continuous synaptic input and thus was at a much more depolarized subthreshold membrane potential than was the case for Mainen et al. (1995).

This cell morphology did not include an axon, so one was created as described in Mainen et al. (1995) and attached to the soma. The axon consisted of an axon hillock 10 μm long with a diameter tapering from 4 to 1 μm that was connected to an initial segment 15 μm long with a diameter of 1 μm. The initial segment was connected to a myelinated axon section followed by a node of Ranvier followed by two more myelinated sections with another node between them. The myelinated sections had lengths of 100 μm and diameters of 1.5 μm, whereas the nodes had lengths of 1 μm and diameters of 1 μm. The axonal membrane capacitance was 0.75 μF/cm^2 on unmyelinated and 0.04 μF/cm^2 on myelinated sections. The axial resistivity of the axon was 200 Ω-cm. Myelinated sections had a membrane leak conductance of 25 μS/cm^2, and all others had a leak conductance of 20 mS/cm^2. The leak reversal potential was -70 mV. The sodium conductance density was 3 mS/cm^2 in the myelinated sections and 3 S/cm^2 in all others. No potassium channels were included in the axon. See Mainen et al. (1995) for a complete description of this axon.

Two forms of the full morphology model were investigated, the high-dendritic-spiking model and the low-dendritic-spiking model. The same morphology was used for both, but a few of their parameters differed. The primary differences were a lower axial resistivity and lower dendritic sodium-conductance density in the dendrites in the low-dendritic-spiking model than in the high-dendritic-spiking model. The low-dendritic-spiking model also had slightly fewer synapses. The relevant parameters for these two models are listed in Table 1. Although we did not attempt to build a complete biophysical model of a CA1 pyramidal neuron, the conductance distributions in the dendrites for the two active conductances included in these models were consistent with experimental findings. In other words, within the apical dendrites, sodium conductance density was constant (Magee and Johnston 1995; Mickus et al. 1999), and persistent potassium conductance density was also constant throughout the dendrites (Chen and Johnston 2004; Hoffman et al. 1997).

Synapses were distributed throughout the apical and basal dendrites of the full morphology models. Action potentials initiated at the axon could backpropagate into the dendrites (the bAPs). In addition, action potentials could be initiated locally within the dendrites. The membrane potential was monitored at the location of every excitatory synapse. Spikes were "detected" by the synapses for the purposes of STDP and anti-STDP whenever the local voltage exceeded −35 mV. To differentiate bAPs from dendritic spikes (solely for display purposes), a spike was counted as a bAP if it arrived at a synapse <20 ms after an action potential was initiated at the axon, otherwise it was counted as a dendritic spike. Although this definition may have misclassified some spikes, experience indicated that these misclassifications were rare and did not alter the conclusions. Both types of spikes had the same effect on synaptic plasticity.

Synapses and synaptic plasticity

Excitatory and inhibitory synapses in all the simulations were activated by presynaptic action potentials generated by independent random Poisson processes at a rate of 10 Hz. Each presynaptic spike activated a synaptic conductance described by a difference of two exponentials with rise time constants of 0.2 and 1 ms and decay time constants of 2 and 8 ms for excitatory and inhibitory synapses, respectively.

TABLE 1. *Parameters for the two versions of the full morphology simulations*

	High-Dendritic-Spiking Full Morphology Model	Low-Dendritic-Spiking Full Morphology Model
Total compartments	961	557
Excitatory synapses	190	170
Inhibitory synapses	38	38
g_{Einitial}	1.0 nS	1.5 nS
g_{I}	0.1 nS	0.1 nS
Axial resistivity	200 Ω-cm	50 Ω-cm
Na^+ conductance density		
Soma:	0.003 S/cm^2	0.003 S/cm^2
Apical:	0.005 S/cm^2	0.0035 S/cm^2
Basal:	0.003 S/cm^2	0.0017 S/cm^2
K^+ conductance density (soma, apical, and basal)	0.01 S/cm^2	0.01 S/cm^2
Leakage conductance density		
Soma:	25 μS/cm^2	25 μS/cm^2
Apical:	50 μS/cm^2	50 μS/cm^2
Basal:	25 μS/cm^2	25 μS/cm^2
Membrane capacitance	0.75 μF/cm^2	0.75 μF/cm^2
Na^+ reversal potential	60 mV	60 mV
K^+ reversal potential	−90 mV	−90 mV
Resting potential	−70 mV	−70 mV

The table does not include axon parameters, which are the same for both models and are given in the text.

Excitatory and inhibitory synaptic currents were defined as $g_{\text{E}}(V - E_{\text{E}})$ and $g_{\text{I}}(V - E_{\text{I}})$, respectively, with $E_{\text{E}} = 0$ mV and $E_{\text{I}} = -70$ mV. The excitatory conductance g_{E} was initialized to a value g_{Einitial} and then was adjusted by the plasticity mechanisms discussed in the following text. The maximal synaptic conductance of inhibitory synapses, g_{I}, was held fixed. For the cylindrical cable, $g_{\text{Einitial}} = 0.65$ nS and $g_{\text{I}} = 0.1$ nS; for the high-dendritic-spiking full-morphology model, $g_{\text{Einitial}} = 1.0$ nS and $g_{\text{I}} = 0.1$ nS; and for the low-dendritic-spiking full-morphology model, $g_{\text{Einitial}} = 1.5$ nS and $g_{\text{I}} = 0.1$ nS. These values were chosen to obtain reasonable postsynaptic firing rates (~10–12 Hz). After the plasticity was activated, simulations were run until maximal synaptic conductances (henceforth called synaptic conductances) reached equilibrium and were no longer modified, other than small, random fluctuations. Plots of synaptic conductance in the figures show $g_{\text{E}}/g_{\text{Einitial}}$.

To implement synaptic plasticity, we computed the interval between every pair of pre- and postsynaptic spikes at a given synapse and defined the interval T as the time of the presynaptic spike minus the time at which the postsynaptic spike reached the synapse. For every pair of spikes, we replaced g_{E} by $g_{\text{E}} + F(T)g_{\text{Einitial}}$ where, for anti-STDP, $F(T) = -A_-\exp(T/\tau_-)$ if $T < 0$ and $F(T) = 0$ if $T \geq 0$, with $A_- = 0.01$ and $\tau_- = 30$ ms. When we implemented STDP, we used $F(T) = A_+\exp(T/\tau_+)$ if $T < 0$ and $F(T) = -A_-\exp(-T/\tau_-)$ if $T \geq 0$, where $A_+ = 0.01$, $A_- = 0.0105$, and $\tau_+ = \tau_- = 20$ ms.

No spike-timing-dependent LTP was included with anti-STDP, but a nonassociative form of LTP was implemented by increasing the weight at a synapse every time a presynaptic spike occurred. Specifically, we replaced g_{E} with $g_{\text{E}} + kg_{\text{Einitial}}$ after each presynaptic spike. For the cylindrical cable model, $k = 0.0024$, and for the full morphology models, $k = 0.004$. This nonassociative LTP is necessary to balance the spike-timing-dependent LTD and equalize synaptic efficacies as detailed in Rumsey and Abbott (2004a).

To measure synaptic efficacy, we computed the cross-correlation function of pre- and postsynaptic action potentials for each synapse while all synapses were being activated by random, Poisson processes. The cross-correlation function was integrated, and the baseline probability was subtracted to obtain the excess pre-before-post spiking probability, which we define as the synaptic efficacy (as in Rumsey and Abbott 2004a).

RESULTS

We explore the effects of anti-STDP as well as STDP in multi-compartment models. The form of anti-STDP used for all of the simulations consists of a presynaptic-before-postsynaptic spike-timing-dependent LTD combined with a nonassociative LTP that depends only on presynaptic spiking (see METHODS). The motivation for this particular combination comes from experiments in the electrosensory system of a weakly electric fish (Bell et al. 1997; Han et al. 2000; Roberts and Bell 2000). For simplicity, we do not include post-before-presynaptic spike-timing-dependent LTP because it is either not present or statistically insignificant in the experimental results (Bell et al. 1997; Han et al. 2000; Tzounopoulos et al. 2004). Including it in our simulations does not change our results (Rumsey and Abbott 2004a).

Cylindrical cable model

The first model we investigated is a cylindrical cable model with active conductances that support the propagation of bAPs from the somatic compartment to the distal end of the cable

(Fig. 1). No action potentials can be initiated within the dendritic cable of this model. All of the synapses initially have the same conductance when activated (Fig. 2*A*). We measured EPSPs for each synapse both at the location of the synapse and at the soma by activating the synapses one at a time. In addition, we determined the efficacy of each synapse, but, in this case, it was done while all of the synapses were being activated randomly. Efficacy for a given synapse is defined as the probability that a presynaptic spike evokes a postsynaptic action potential that arrives at the site of that synapse. This definition is slightly different from efficacy as conventionally defined to reflect merely the number of axonal spikes induced by the activity of a synapse.

The initial dendritic and somatic EPSP amplitudes from this model are shown in Fig. 2*C.* The initial efficacies (Fig. 2*E*) are much higher for proximal than for distal synapses as would be expected. After plasticity has been active for a sufficient length of time, the maximal synaptic conductances come to equilibrium at a point where the synaptic efficacies have been equalized (Fig. 2*F*). Efficacy equalization requires a distance-dependent scaling of synaptic conductances in which the proximal synapses have been weakened and the distal synapses have been strengthened (Fig. 2*B*). This produces final dendritic EPSP amplitudes (Fig. 2*D,* red dots) that increase with distance from the soma and somatic EPSP amplitudes (Fig. 2*D,* blue dots) that also increase slightly. Notably, the somatic EPSPs are equalized for the first few hundred micrometers from the soma, similar to the equalization of somatic EPSP amplitudes found experimentally in CA1 pyramidal neurons (Magee and Cook 2000). The results shown in Fig. 2 closely resemble the high-conductance, passive cable simulation in Rumsey and Abbott (2004a). Thus the inclusion of bAPs does not prevent or alter the equalization of synaptic efficacies by anti-STDP.

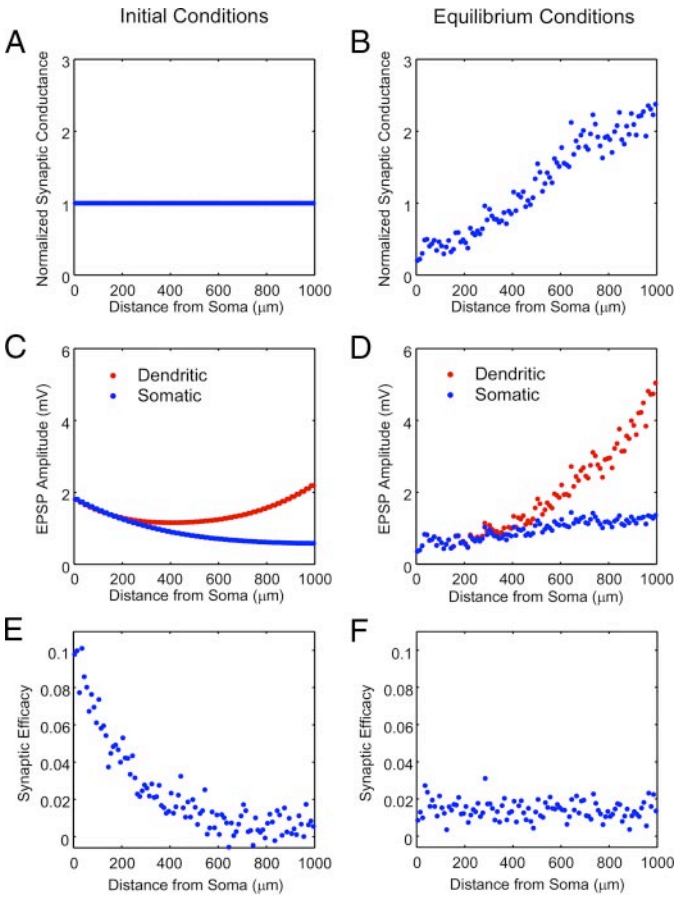

FIG. 2. Anti-spike-timing-dependent plasticity (anti-STDP) in an active cylindrical cable model. Each dot represents the value for a given excitatory synapse, and all plots show synapses as a function of their distance from the soma. *Left*: initial conditions; *right*: final equilibrium state. *A*: initially, all the synapses have the same (maximal) synaptic conductance, which has been normalized for the plots to the value 1. *B*: after anti-STDP has acted long enough to attain a stable equilibrium distribution of synaptic conductances, proximal synapses are weakened and distal synapses strengthened, resulting in a distance-dependent increase in synaptic conductance. *C*: initial, local dendritic excitatory postsynaptic potential (EPSP) amplitudes (red dots) and corresponding EPSP amplitudes at the soma (blue dots). Somatic EPSP amplitude decreases with distance. *D*: equilibrium dendritic EPSP amplitudes (red dots) grow with distance, whereas somatic EPSP amplitudes (blue dots) show approximate equalization. *E*: initial synaptic efficacy, defined as the probability of a presynaptic spike at the given synapse evoking a postsynaptic action potential, decreases strongly with distance from the soma. *F*: equilibrium synaptic efficacies have all been equalized by anti-STDP.

CA1 pyramidal morphology models

The active cylindrical cable provides a first step, but, to further explore the effects of anti-STDP, we used an actual morphology. The morphology used for these simulations is a reconstructed CA1 pyramidal neuron (Fig. 3*A*). An axon has been added for generating postsynaptic action potentials that backpropagate into the apical and basal dendrites due to the presence of voltage-dependent dendritic Na^+ and K^+ conductances (described in METHODS). Synapses are located throughout the apical and basal dendrites (Fig. 3*B*) and, as in the cylindrical cable, plasticity mechanisms are activated when action potentials reach the synapse. Postsynaptic spiking is driven entirely by the synaptic input.

Figure 3*C* shows an example of a bAP in this model. Including these conductances also allows us to consider the initiation of action potentials locally within the dendrites. Some of these dendritically generated spikes propagate to the soma and successfully initiate action potentials at the axon, while others do not. In the following, we call action potentials initiated in the dendrites dendritic spikes whether or not they propagate to the soma and become axonal spikes. Action potentials that invade the dendrites after being initiated in the soma or axon are called backpropagating or bAPs. Here synaptic efficacy refers to the likelihood that activating a synapse induces either a bAP or a dendritic spike that then invades the synapse.

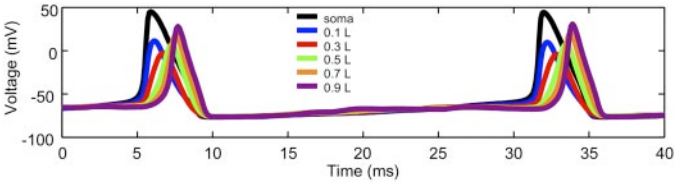

FIG. 1. Backpropagating action potentials (bAPs) in an active cylindrical cable. Two bAPs are shown. *L*, total length of the cable (1,000 μm). Each color is a measure of the membrane potential at the indicated distance from the soma. As in the simulation, these bAPs were initiated by random synaptic activity.

The first version of this model that we analyze is referred to as the high-dendritic-spiking model because, in its initial state, it is particularly prone to generating spikes within the dendrites. The synaptic conductances and EPSPs for this model are

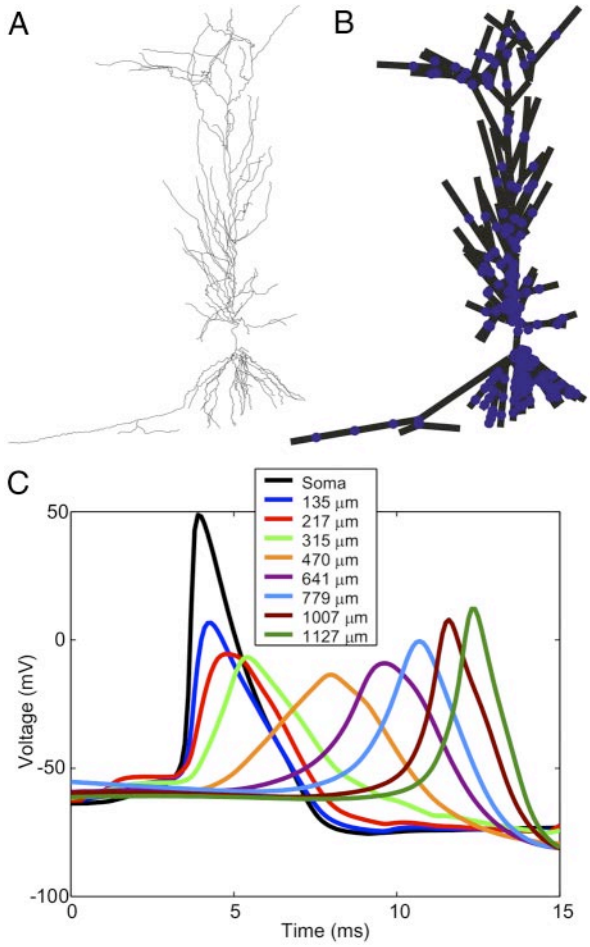

FIG. 3. CA1 pyramidal neuron morphology and backpropagating action potential. *A*: reconstructed CA1 pyramidal neuron morphology (*n123* from the Duke/Southampton Archive of Neuronal Morphology). This is the neuron used for all of the full morphology simulations described. *B*: synaptic placement in one of the neuronal morphology models. In this schematic of the neuron shown in *A*, dots correspond to the locations of the 190 excitatory synapses used in the high dendritic spiking model. *C*: bAP in a full morphology model. This is an example of a bAP propagating from the soma through the main apical shaft and to the most distal branch. Distances correspond to the path distance along the dendrites from the soma.

shown in Fig. 4. In all figures, results are plotted as a function of the path length (in micrometers) along the dendritic tree from the soma to the synapse (not the straight-line distance between the soma and the position of the synapse). In the simulation shown in Fig. 4, 190 excitatory synapses were initialized to the same synaptic conductance (Fig. 4*A*). A first indication of why this version is called the high-dendritic-spiking model can be seen in the plot of initial dendritic EPSP amplitudes (Fig. 4*C*). EPSPs for three of the synapses are above threshold for initiating a dendritic spike. Figure 4*E* shows the steep decrease with distance of the initial somatic EPSP amplitudes.

To investigate synaptic equalization, we activated anti-STDP and ran the simulation until the synaptic conductances reached equilibrium. An examination of the equilibrium synaptic conductances and EPSP amplitudes in this model does not appear particularly revealing inasmuch as it does not resemble the equilibrium state of the cylindrical cable model (Fig. 2). The final synaptic conductances show no overall trend or scaling with distance from the soma (Fig. 4*B*). The three EPSPS that were originally suprathreshold for dendritic spikes are now subthreshold (Fig. 4*D*), but the final somatic EPSP amplitudes (Fig. 4*F*) still show a strong decrease with distance. It is not immediately apparent what, if anything, anti-STDP has accomplished in this model.

Part of the answer, however, can be found in the results of Fig. 5, which breaks down the types of action potentials seen by each synapse. Every time an action potential is registered at a particular synapse, it is classified as either a bAP or a dendritic spike (see METHODS). Figure 5*A* shows the total firing rate for bAPs and dendritic spikes together observed at each synapse. The line indicates the postsynaptic firing rate for axon-generated action potentials alone. Clearly, many synapses in this model see a high number of locally-generated dendritic spikes, which is further illustrated by the breakdown between bAPs and dendritic spikes in Fig. 5, *C* and *E*. Figure 5*C* shows the number of bAPs that successfully reach each synapse as a percentage of the total number of axonal action potentials. Only the most proximal synapses receive 100% of the back-propagating spikes. Failures in backpropagation increase more distally, so that the most distal synapses receive only ~45% of the bAPs. Figure 5*E* plots the percentage of action potentials registered at each synapse that are of dendritic origin. In this

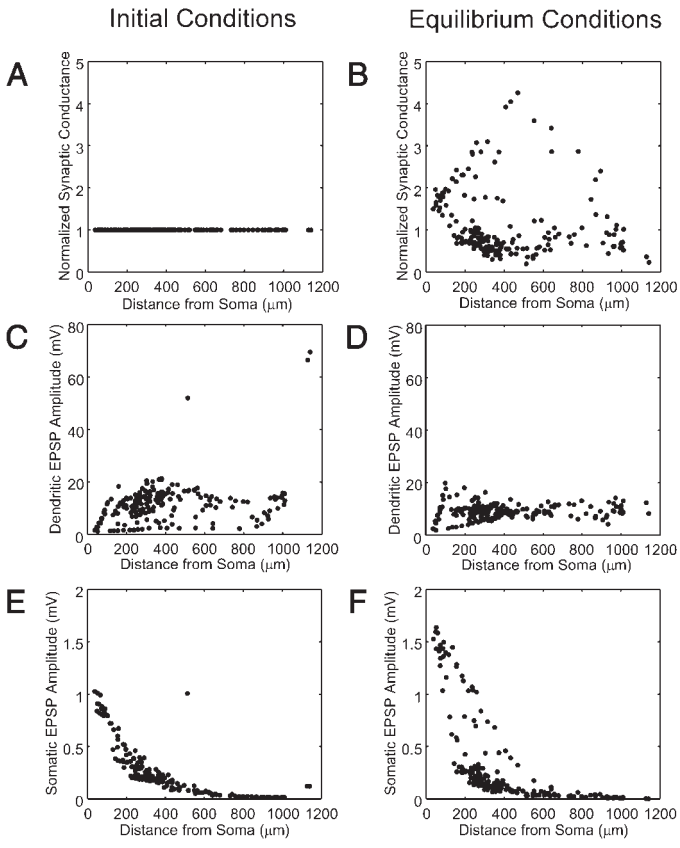

FIG. 4. Synaptic conductances and EPSP properties in a high-dendritic-spiking model. Synapses are arranged in order of their dendritic path distance from the soma. *A*: all synapses initially have the same conductance. *B*: final distribution of synaptic conductances. *C*: initial dendritic EPSP amplitudes. Three of the EPSPs result in dendritic action potentials, giving them very large amplitudes. *D*: final dendritic EPSP amplitudes in which suprathreshold EPSPs are no longer present. *E*: initial somatic EPSP amplitudes. *F*: final somatic EPSP amplitudes.

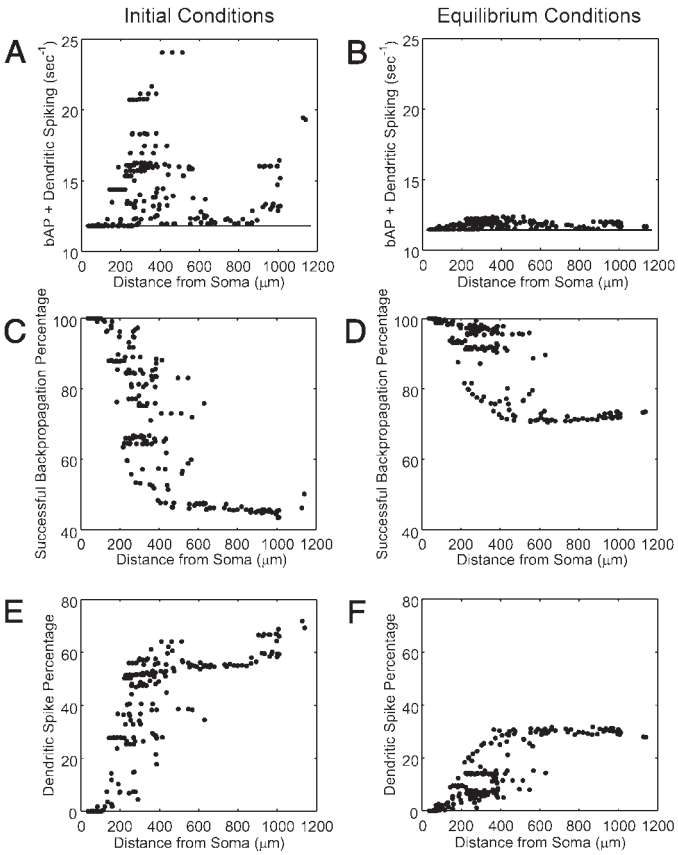

FIG. 5. Counts of backpropagating and dendritically initiated spikes in a high-dendritic-spiking model. *A*: combined spiking rate for bAPs and dendritic spikes that reach each synapse is plotted as a function of the dendritic path length from the synapse to the soma, under the initial conditions of the model when all synapses have the same conductance. —, firing rate of the axon. Some synapses see a much higher firing rate due to the amount of dendritic spiking. *B*: combined spiking rate at equilibrium after anti-STDP has modified synaptic conductances. In this condition, all synapses experience approximately the same frequency of postsynaptic spiking. *C*: initial percentage of action potentials initiated at the axon that successfully backpropagate to each synapse. *D*: percentage of successful bAPs is increased by anti-STDP. *E*: initial percentage of spikes detected by each synapse that are classified as dendritic spikes. *F*: percentage of dendritic spiking at equilibrium is reduced.

case, the more proximal synapses see few dendritic spikes, whereas ~70% of the spikes appearing at the most distal synapses are dendritic.

The initial state of this model produces a high level of dendritic spiking. The final, equilibrium results from Fig. 5, however, reveal a striking consequence of anti-STDP. At equilibrium, the reliability of backpropagation from the axon has been substantially improved (Fig. 5*D*). Even the most distal synapses receive >70% of the bAPs. At the same time, dendritic spiking has been substantially reduced so that only ~30% of the action potentials arriving at the distal synapses originate in the dendrites (Fig. 5*F*). Even more remarkably, the failure of backpropagation at large distances from the soma is compensated by an increase in dendritic spiking, so spikes arrive at the same rate at any point along the dendritic cable (Fig. 5*B*). In other words, at equilibrium, each synapse receives postsynaptic spikes at about the same rate regardless of its location, but the ratio of dendritic to back-propagating spikes increases along the dendrite. Thus anti-STDP not only regulates dendritic spiking, it also normalizes the total level of postsynaptic spiking seen throughout the entire dendritic tree.

In this particular model, the major part of this compensation results from the fact that dendritic spikes that reach the axon induce a bAP that propagates elsewhere in the dendrites but not to those dendrites from which it originated. This is a consequence of the Na^+ inactivation that follows the dendritic spike, which blocks the subsequent bAP from entering that part of the dendrite, a finding that matches experimental results in CA1 pyramidal neurons (Golding and Spruston 1998). For instance, a dendritic spike initiated in the distal apical dendrite that travels down the apical tree to the soma will initiate an action potential at the axon. This spike will then invade the basal dendrites but will not propagate back into the apical tree where the Na^+ channels were just inactivated, ensuring that the dendritic spike detected by the apical synapses is matched with a bAP detected by the basal synapses. The remainder of the compensation for bAP failures comes from localized dendritic spikes that do not reach the axon.

Why did anti-STDP have this consequence? As in the cylindrical cable model, anti-STDP equalizes synaptic efficacies, but now synaptic efficacy refers to both the probability of evoking a back-propagating action potential and also the likelihood of inducing a dendritic spike. Thus by equalizing all the synaptic efficacies, anti-STDP normalizes postsynaptic spiking (Roberts 2000; Rumsey and Abbott 2004a; Williams et al. 2003). Figure 6*A* shows the initial synaptic efficacies for the high-dendritic-spiking model. Some of the values in this plot indicate synapses that have extremely high synaptic efficacies because, very often, activating them results in a dendritic spike. By equalizing the efficacies (Fig. 6*B*), anti-STDP prevents these synapses from having any greater likelihood of inducing a dendritic spike than other synapses have at inducing a bAP. The relationship between dendritic spiking and synaptic efficacy has also been explored in previous theoretical work (Rudolph and Destexhe 2003).

To further explore the action of anti-STDP in morphologically accurate models and to ascertain the robustness of the above findings, we altered the parameters of the high-dendritic-spiking model to create a qualitatively different initial model (Table 1). The new model, called the low-dendritic-spiking model, was designed to minimize initial dendritic spiking.

The initial synaptic conductances for the low-dendritic-spiking version are all equal (Fig. 7*A*) and, in contrast to the high-dendritic-spiking model, none of the initial dendritic

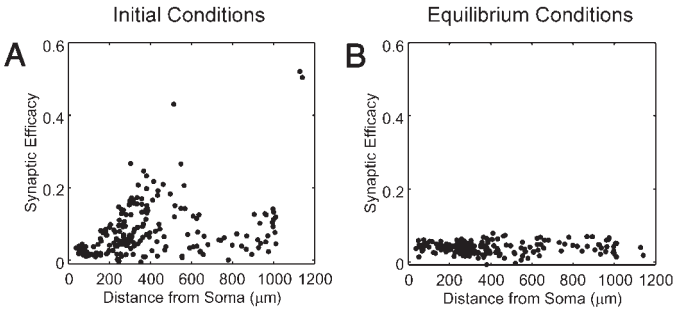

FIG. 6. Synaptic efficacies in a high-dendritic-spiking model. The calculation of synaptic efficacy counts both bAPs and dendritic spikes equally. *A*: initial efficacy of each synapse is shown. Particularly high values correspond to a high probability of inducing a dendritic spike near the synapse. *B*: anti-STDP equalizes the synaptic efficacies.

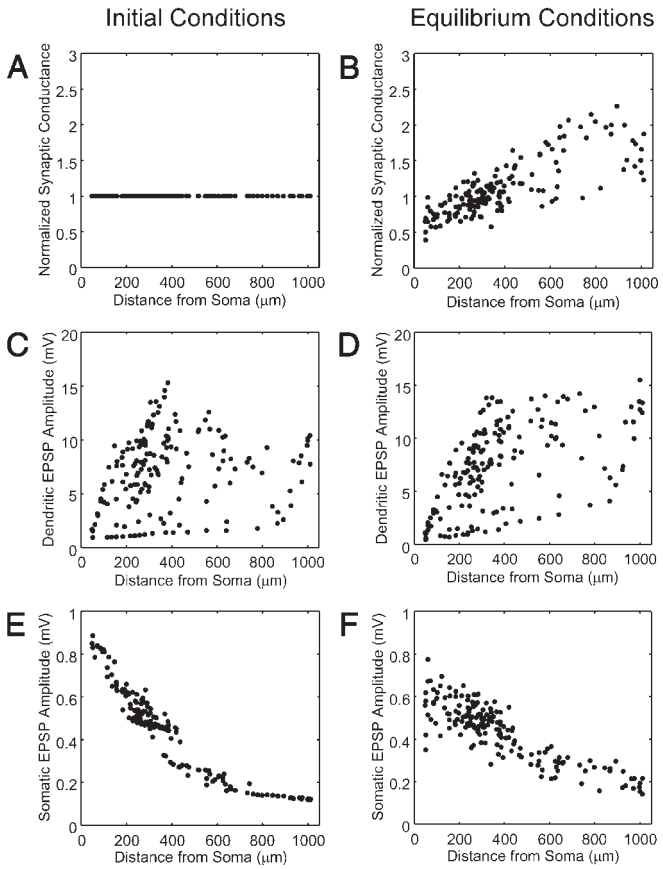

FIG. 7. Synaptic conductances and EPSP properties in a low-dendritic-spiking model. *A*: initial synaptic conductances. *B*: at equilibrium, synaptic conductances display a distance-dependent increase. *C*: initial dendritic EPSP amplitudes. *D*: dendritic EPSP amplitudes after anti-STDP. *E*: initial somatic EPSP amplitudes decrease with distance from the soma. *F*: equilibrium somatic EPSP amplitudes do not decrease as much and are equalized to ~400 μm from the soma.

EPSP amplitudes (Fig. 7*C*) of this model is suprathreshold. The initial somatic EPSP amplitudes (Fig. 7*E*) decrease with distance from the soma as they did in the high-dendritic-spiking model. However, in this model, the equilibrium synaptic conductances now show a distance-dependent increase (Fig. 7*B*) similar to that in the cylindrical cable model. The dendritic EPSP amplitudes increase with distance as well but are much more dispersed here (Fig. 7*D*). Interestingly, the somatic EPSP amplitudes at equilibrium are equalized out to ~400 μm from the soma (Fig. 7*F*) as they were for the cylindrical cable and also as is seen experimentally (Magee and Cook 2000).

How do the relative numbers of bAPs and dendritic spikes in this version compare with the high-dendritic-spiking model? The initial state of this model shows little dendritic spiking (Fig. 8, *left*). Very few of the synapses see any dendritic spikes, and those that do see very few (Fig. 8*E*). No more than 1% of the total spikes at these synapses are dendritic in origin. As Fig. 8*C* shows, backpropagation of action potentials from the soma is initially 100% successful for almost all of the synapses with very few failures for the others. The bAPs invade the dendrites more successfully in this model than they did in the previous model even though the previous model had a higher excitability because, as mentioned previously, high dendritic spiking in the previous model led to more Na^+ inactivation, which blocked bAPs in that model. Initially, the combined spiking rate due to both bAPs and dendritic spikes is essentially the same across all the synapses with no greater than approximately a 0.1-Hz difference between any two synapses (Fig. 8*A*). Contrast this with Fig. 5*A* from the high-dendritic-spiking model in which the spread is >10 Hz.

Starting from this initial configuration, anti-STDP increases the conductance of the more distal synapses relative to the more proximal ones (Fig. 7*B*). The increase in distal synaptic strength leads to an increase in the number of distal dendritic spikes (Fig. 8*F*), so that now ~8% of the action potentials at the most distal synapses are dendritic. This increase in dendritic spiking leads to more failures of bAPs for the more distal synapses (Fig. 8*D*). The percentage of successful backpropagation drops from 100% initially to ~92% for the most distal synapses at equilibrium. Consequently, the combination of bAPs and dendritic spikes is as flat across the dendritic tree (Fig. 8*B*), differing by no more than ~0.1 Hz, as it was initially (Fig. 8*A*). Although in the high-dendritic-spiking model, both backpropagation failures and dendritic spiking decreased as a result of anti-STDP and in the low-dendritic-spiking model, both backpropagation failures and dendritic spiking increased,

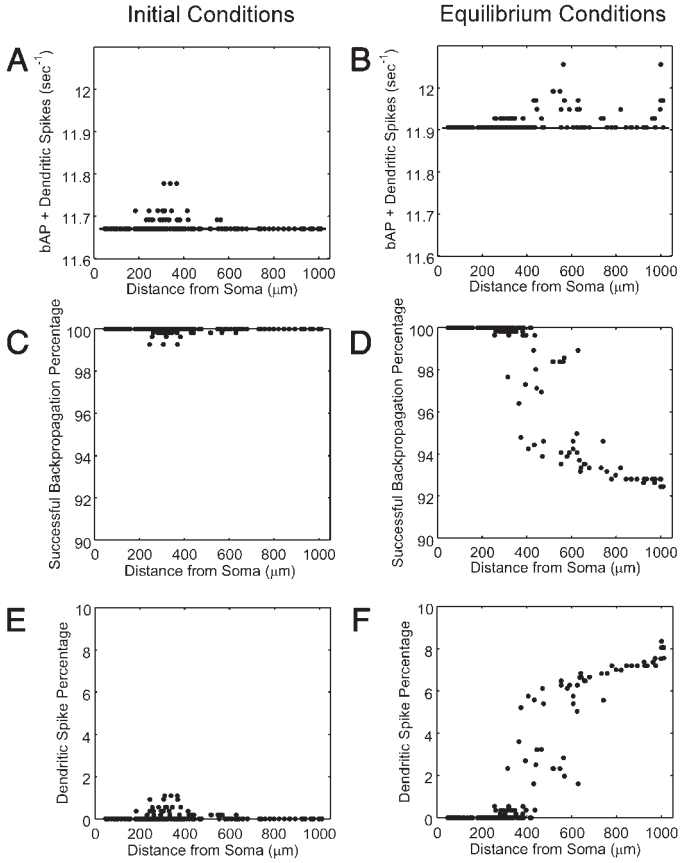

FIG. 8. Backpropagating and dendritic spike counts in a low-dendritic-spiking model. *A*: combined bAP and dendritic spike postsynaptic firing rate experienced by each synapse when all synapses have the same conductance. —, firing rate of the axon. *B*: combined firing rate at equilibrium is quite similar to that shown in *A* with just a slight increase in the axonal firing rate. *C*: initially there are almost no failures of backpropagation in the dendrites. *D*: anti-STDP leads to an increase in the number of failures (though still much less than in the high dendritic spiking model). *E*: initially there are almost no dendritic spikes in this model. *F*: anti-STDP leads to an increase in dendritic spiking but again much less than in the high-dendritic-spiking model.

the net effect in both models is a regulation of the total rate of spiking.

The reasoning is the same for the low-dendritic-spiking model as it was for the high-dendritic-spiking model. The initial synaptic efficacy in the low-dendritic-spiking model more closely resembles that from the cylindrical cable simulations in its clear decrease with distance from the soma because it lacks dendritic spiking (Fig. 9*A*). At equilibrium, the synaptic efficacies have been equalized as in all the previous simulations (Fig. 9*B*), which gives rise to the same regulation of spiking, although achieved in a slightly different manner than in the high-dendritic-spiking case.

In both the equalized high- and low-dendritic-spiking models, most of the synapses help produce somatic spikes, some through somatic EPSPs and others through dendritic spikes that propagate to the soma. What occurs in a model in which a subset of synapses is largely cut off from activity in the rest of the cell? To answer this question, we investigated a variant of the low-dendritic-spiking model. The parameters of this variant, referred to here as the multiple domain model, were identical to those of the low-dendritic-spiking model with the one exception that the axial resistivity of the apical dendrites was set to 200 Ω-cm (the same value used for all of the dendrites in the high-dendritic-spiking model). This had the effect of creating two different domains. In one domain, consisting of the basal dendrites, soma, and proximal apical dendrites, dendritic spiking was negligible and backpropagation of action potentials was nearly perfect (as in the low-dendritic-spiking model). In the distal apical dendrites, however, dendritic spiking dominated (as in the high-dendritic-spiking model). These dendritic spikes did not often reach the soma, and bAPs did not frequently reach the distal synapses.

The effects of anti-STDP in this model reflect the outcomes observed in both the low- and high-dendritic-spiking models. The proximal synapses are modified in this model as were all the synapses in the low-dendritic-spiking model (i.e., distance-dependent synaptic conductances), and the distal apical synapses are modified as all the synapses were for the high-dendritic-spiking model (i.e., regulation of dendritic spiking). Because the data for this model simply reflect the figures already shown, they are not displayed. The important result is that its two functionally separate domains are equalized independently, although by different means. The synaptic efficacies within each domain are equalized, and the spiking rate in each domain is regulated.

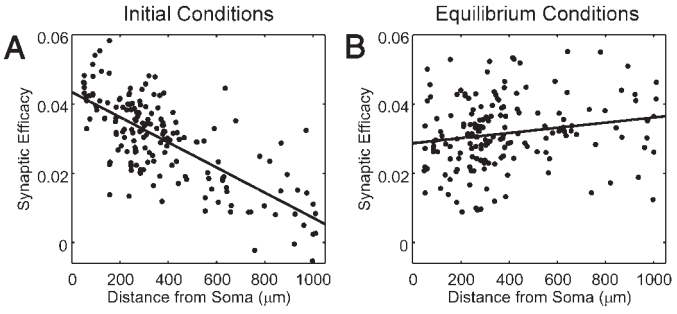

FIG. 9. Synaptic efficacies in a low-dendritic-spiking model. —, straight line fits to the data. *A*: initial synaptic efficacies decrease with distance from the soma (correlation coefficient: $R = -0.72$). *B*: anti-STDP equalizes synaptic efficacies ($R = 0.18$).

Synaptic equalization and STDP

We now turn from our studies of anti-STDP to consider the effects of STDP, in which pre-before-postsynaptic spiking generates LTP and post-before-presynaptic spiking generates LTD, in extended multi-compartment neuron models. Most computational studies of STDP have considered single-compartment models and not investigated its action in multi-compartment models. What are the consequences of STDP in models with complex morphology?

To answer this question, we used the same models explored in the preceding text again but subjected the excitatory synaptic conductances to STDP (described mathematically in METHODS) rather than anti-STDP. The model of STDP we use in this study is intrinsically unstable (Song et al. 2000). This instability is what drives learning in such models, but it also makes them prone to domination by locally generated action potentials (Goldberg et al. 2002). Other more stable models of STDP have been developed (Gütig et al. 2003; Rubin et al. 2001; van Rossum et al. 2000). Synapses subject to such forms of plasticity are sensitive to correlations in presynaptic input patterns but cannot retain traces of these correlations once they have been removed. Because such models are less prone to the problem we are discussing, although not immune to it, we restrict our analysis to the less stable form of STDP. Solving the problem in this worst-case scenario is sufficient to show that it can be solved for the more stable forms of plasticity as well.

The instability discussed in the preceding text requires us to place bounds on the synaptic conductances when we introduce STDP. Specifically, synaptic conductances were not allowed to potentiate to >1.5 times their initial value or to depress to a value <0. As in the previous simulations, the synaptic conductances all start out with the same value (Fig. 10, *left*). Synaptic inputs were then activated as before, and STDP modified synaptic conductances.

In the high-dendritic-spiking model, most of the synapses get potentiated by STDP to their upper limit (Fig. 10*B*). It is not surprising that Hebbian plasticity leads to trouble in the presence of a high degree of dendritic spiking. Synapses correlated with a large degree of dendritic spiking get potentiated, leading to even more dendritic spiking and so on. The resulting positive feedback loop forces synapses to their maximum strength, and postsynaptic activity quickly gets out of control. The few synapses that escape this fate are located on branches or regions of the dendritic tree that do not support much dendritic spiking, and these get depressed and effectively shut down. This scenario was described by Goldberg et al. (2002).

Synaptic fate is not much improved in the low-dendritic-spiking model, although the outcome is different (Fig. 10, *C* and *D*). In the initial state of this model (Fig. 10*C*), dendritic spiking does not occur. As shown in Fig. 10*D,* STDP potentiates all of the proximal synapses and depresses all the distal synapses. This is due to the decrease in synaptic efficacy with distance from the soma in this model (Fig. 9*A*). The more attenuated distal input cannot compete successfully with the higher efficacy proximal input so the competitive STDP rule strengthens the proximal synapses at the expense of the distal synapses.

The same outcome applies to the cylindrical cable model (Fig. 10, *E* and *F*). In this case, it is even more obvious that the

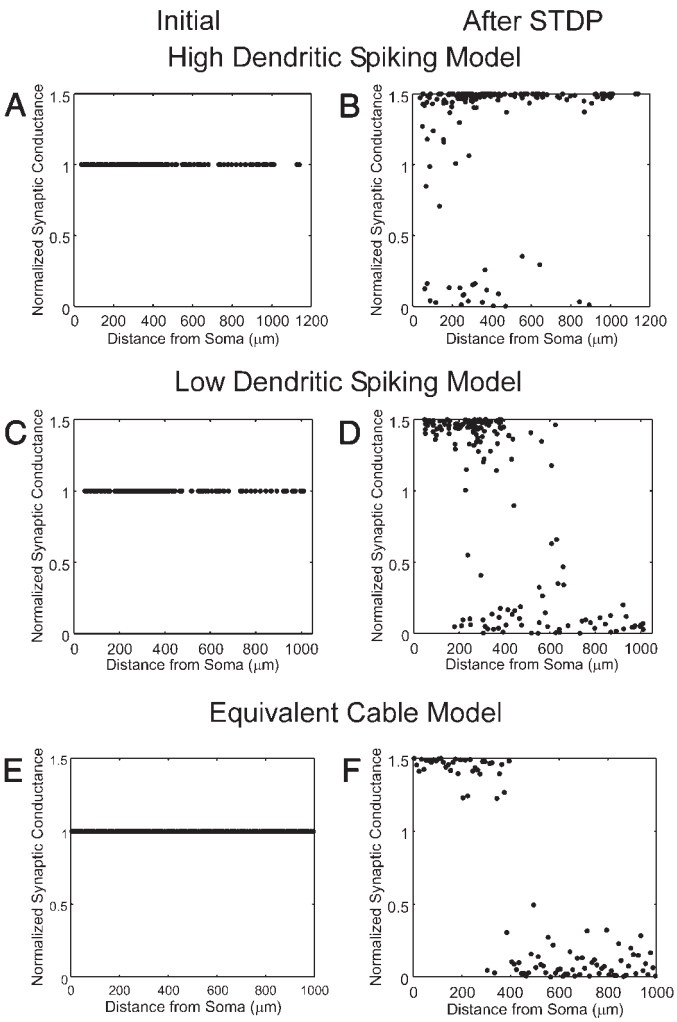

FIG. 10. STDP in 3 models. In each case, synapses are initialized to the same conductance. Also in each case, there is a maximum limit on synaptic conductance to preclude potentiation beyond 1.5 times the starting value and a minimum limit to prevent synaptic conductances below 0. *A*: initial synaptic conductances in the high-dendritic-spiking model. *B*: STDP causes most of the synapses to be potentiated in the high-dendritic-spiking model. *C*: initial conductances in the low-dendritic-spiking model. *D*: STDP causes the proximal synapses to be potentiated and the distal synapses to be depressed in the low-dendritic-spiking model. *E*: initial conductances in the cylindrical cable model. *F*: as in *D,* STDP potentiates the most proximal synapses at the expense of the more distal synapses in a cylindrical cable model.

few most proximal synapses out-compete the more distal synapses for potentiation by STDP (Fig. 10*F*).

How might this situation be rectified and these disasters avoided? STDP magnifies differences in synaptic efficacy, whereas anti-STDP removes such differences. Therefore if different synaptic efficacies are first equalized by anti-STDP, then STDP can be used to select relevant inputs without undue bias resulting from synapse location. This sequence is shown in Fig. 11 for the active cylindrical cable. After anti-STDP has equalized synaptic efficacies, all synapses have an equal likelihood of being potentiated or depressed regardless of their position. For this simulation, the upper limit on synaptic conductance for the STDP portion of the sequence is set equal to twice the value of the synaptic conductance attained by anti-STDP, which implies a distance-dependent limit. This assures that the synapses maintain an equal average efficacy even after they are potentiated by STDP. An adjustable limit like this can arise quite naturally. For example, if anti-STDP controls the number of receptors at a synapse and STDP modulates the open conductance of those receptors, the upper limit on synaptic strength will be proportional to the value established by anti-STDP as we have assumed.

The distribution of synaptic conductances shown in Fig. 11*D* is quite similar to the distribution observed experimentally in CA1 pyramidal neurons. In these cells, only a fraction of the synapses are scaled with distance; the remainder have equally low efficacies regardless of their distance from the soma (Andrásfalvy and Magee 2001; Magee and Cook 2000; Smith et al. 2003). This is mirrored in Fig. 11*D,* which shows that STDP, acting after anti-STDP, creates a subset of synaptic conductances scaled with distance and a subset that have equally small synaptic conductance regardless of distance.

DISCUSSION

Anti-STDP combined with nonassociative potentiation equalizes synaptic efficacies in passive, active, and branched multi-compartment models, providing a powerful homeostatic mechanism for establishing a dendritic democracy in which the influence of a synapse is independent of its location. Anti-STDP equalizes efficacies in active cables that include bAPs and in models with CA1 pyramidal neuron morphologies that support dendritic spike initiation. The effect of efficacy equalization occurs because a synapse that is too weak to affect the postsynaptic response is not much modified by the pre-before-

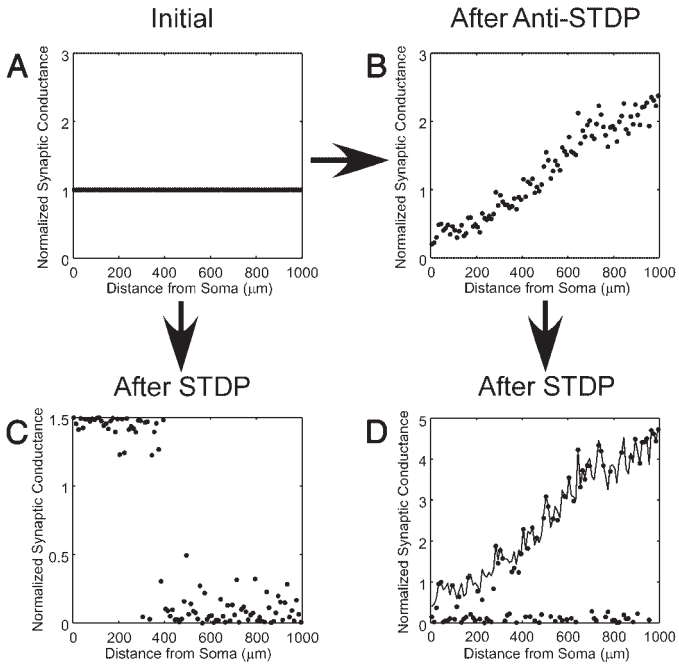

FIG. 11. STDP in an equalized, active cylindrical cable model. *A*: in the initial cable, all synapses have the same conductance and an unequal distribution of synaptic efficacies. *B*: distribution of synaptic conductances if anti-STDP is first allowed to modify the synapses and equalize the synaptic efficacies. *C*: distribution of synaptic conductances if only STDP acts on the initial distribution in *A*. *D*: if STDP follows after equalization by anti-STDP, proximal synapses have no advantage over distal synapses and STDP randomly potentiates and depresses synapses along the entire length of the cable. —, upper limit that is set on synaptic conductance for STDP. It is set to twice the value of the equilibrium conductance determined by anti-STDP in *B*.

post, spike-timing-dependent LTD of anti-STDP but rather tends to be strengthened by the nonassociative potentiation. On the other hand, a synapse that has too high a synaptic conductance gives rise to many bAPs and/or dendritically generated spikes and so takes part in many LTD interactions and thus is weakened. These two processes continue until the LTP just balances with and cancels the LTD, and this occurs at a specific value of synaptic efficacy that is the same for all synapses (Roberts and Bell 2002; Rumsey and Abbott 2004a,b).

Our computational results indicate that anti-STDP is a plausible mechanism to explain the location independence of synapses observed in the various experimental preparations. In the cylindrical cable and low-dendritic-spiking models, equalization of synaptic efficacies is achieved through distance-dependent scaling of synaptic conductances, similar to what is observed experimentally in CA1 pyramidal neurons (Andrásfalvy and Magee 2001; Magee and Cook 2000; Smith et al. 2003). From the soma out to ~400 μm, scaling equalizes somatic EPSP amplitudes, as reported in several preparations (Andersen et al. 1980; Iansek and Redman 1973; Jack et al. 1981; Magee and Cook 2000; Stricker et al. 1996). However, somatic EPSPs are not location independent in the high-dendritic-spiking model. It may be that biological CA1 pyramidal excitability more closely resembles that of the low-dendritic-spiking model in which dendritic spikes are more difficult to initiate, requiring stronger coincident local input, for instance. If so, then, as our low-dendritic-spiking model results indicate, equalizing synaptic efficacy by anti-STDP can equalize somatic EPSPs. Additionally, the experimental dendritic measurements do not extend all that far out, leaving the distance unknown over which somatic EPSPs are location-independent.

Actually, anti-STDP is an even more powerful mechanism as seen in models with CA1 pyramidal morphology. Goldberg et al. (2002) suggested previously that an anti-Hebbian plasticity rule might be an effective means of normalizing dendritic spiking and preventing explosive potentiation of synapses in "hot" regions of the dendrite by Hebbian plasticity. Indeed, anti-STDP normalizes dendritic spiking, balancing it with the level of spiking due to backpropagation from the soma and preventing runaway spiking in localized dendritic regions. Anti-STDP ensures that every synapse receives postsynaptic spikes at about the same rate (Roberts 2000; Rumsey and Abbott 2004a; Williams et al. 2003). Whether the firing rate at any particular synapse consists primarily of bAPs or dendritic spikes or involves a mixture of the two depends on its location, but the total rate is roughly the same at all synapses. This finding is consistent with previous theoretical work showing that an anti-STDP learning rule regulates the postsynaptic rate due to a stable fixed point in the learning dynamics (Roberts 2000; Williams et al. 2003).

STDP can create a positive feedback loop so that dendritically generated spikes lead to stronger synapses, which in turn generate more dendritic spikes. If this occurs, some dendritic branches or regions dominate the neuronal response, whereas branches that lack dendritic spiking are entirely shut down (Goldberg et al. 2002). Anti-STDP provides a potent regulatory mechanism for avoiding such an outcome.

Of course, a perpetual state of equalization is not necessarily the goal of plasticity. The real benefit of anti-STDP is to set a stage in which every synapse has an equal opportunity to play a role in postsynaptic processing without being either advantaged or disadvantaged purely on the basis of synaptic placement. Anti-STDP removes these location-dependent biases and puts the synapses on an equal footing for Hebbian plasticity to then select synapses for potentiation or depression on a functional basis.

These observations suggest that anti-STDP may be an important developmental mechanism. In one scenario, anti-STDP would only be present during a particular developmental phase. Then later in development, STDP would be activated, allowing for Hebbian learning. However, given the continual need to maintain a normalizing, homeostatic force to counterbalance Hebbian processes, anti-STDP may operate continuously even in the adult, but anti-STDP may be a much slower process, responding only over long time scales. It is also conceivable that the two forms of plasticity may cycle between one another, for example during sleep and wakefulness.

If any of these scenarios is correct, it might explain why anti-STDP has not been previously observed in cells such as CA1 pyramidal neurons that exhibit distance-dependent synaptic scaling. If anti-STDP is a slow process or only present at a particular developmental stage, it could have been missed in experiments. As the computational results make clear, anti-STDP could provide a powerful and elegant solution for explaining the experimental results as well as some of the basic problems associated with applying Hebbian plasticity to extended neurons.

Additionally, recent experimental results on STDP may indicate a further need for a homeostatic anti-STDP process. Froemke et al. (2005) found that in cortical layer 2/3 pyramidal neurons, the temporal windows for STDP vary along the apical dendrite with distance from the soma such that the timing window for LTD increases more distally. This would seem to place distal synapses at even more of a disadvantage in terms of their competition with proximal synapses. Anti-STDP may provide a mechanism for maintaining these distal synapses in the face of added pressures for elimination.

We have not attempted to model a realistic distribution of active conductances in our CA1 pyramidal morphology models. The range of channel types found in the dendrites of real CA1 pyramidal neurons is extensive (Johnston et al. 1996). Our goal was to include enough conductances, arranged in the proper distribution, to achieve axonal initiation and successful backpropagation of action potentials and dendritic spike initiation in the presence of random background synaptic activity. Changing the number, types, or specific distributions of channels in the neuron would alter the values of the initial synaptic efficacies, the initial extent of the backpropagation of spikes, and the initial numbers and locations of dendritic spike initiations and would lead to different equilibrium synaptic conductances. Nevertheless, the end result would be the same: anti-STDP would equalize the synaptic efficacies and would regulate dendritic spiking and eliminate the location dependence of the synapses. That is, in fact, one of the primary benefits of using such an anti-STDP mechanism to equalize synapses: it does not depend on whatever specific morphology or conductance profile exists between a given synapse and a site of action potential generation. A different distribution of synaptic conductances may be required to achieve equalization under a different conductance profile, but equalization will still be achieved. The differences between the high-dendritic-spiking

model and the low-dendritic-spiking model provide an example of this.

Indeed, the high- and low-dendritic-spiking models represent the extreme cases. In the high-dendritic-spiking model, dendritic spikes are far more prevalent and easy to initiate than is realistic. In the low-dendritic-spiking model, on the other hand, backpropagation of action potentials from the soma/axon is much stronger than is realistic. Yet in both cases, anti-STDP is successful in equalizing the synapses and acts to move the models away from the extremes. As mentioned in RESULTS, a third model was investigated that was more intermediate and contained attributes of both the high- and low-dendritic-spiking models. The results of anti-STDP in this intermediate model reflected aspects of the results shown for both the high- and low-dendritic-spiking models. Anti-STDP is capable of equalizing synapses over wide range of operating regimes.

Anti-STDP operating on synaptic conductances is unlikely to be the only means by which a neuron regulates its spiking. Activity-dependent modification of active conductances in the dendrites likely plays a role in these phenomena as well. For example, in some cases, equalizing synaptic efficacies and normalizing spiking levels may not be possible within a realistic range of synaptic conductances. This is presumably the point at which homeostatic plasticity of active channel distributions would come into play (Siegel et al. 1994). In general, anti-STDP must interact with other forms of homeostatic plasticity including nonsynaptic, indirect, and global synaptic mechanisms (Turrigiano and Nelson 2004). On the other hand, these other forms of homeostatic plasticity acting in the absence of anti-STDP are unlikely to be capable of achieving the same end results described here. A major benefit of anti-STDP is its synapse specificity. Other forms may be able to regulate global efficacy, but anti-STDP is able to regulate efficacy on a synapse-by-synapse basis. Rabinowitch and Segev (2006) provide a further investigation of this issue.

All of the simulations examined here treated dendritic spikes as indistinguishable from bAPs from the point of view of the synapses. It is possible that synapses can distinguish between the two and respond to them differently. In CA1 and cortical pyramidal neurons, bAPs are Na^+ spikes, but dendritic action potentials can be Na^+ and/or Ca^{2+} spikes (Golding and Spruston 1998; Golding et al. 1999; Häusser et al. 2000; Schiller et al. 1997). As such, bAPs and dendritic spikes could potentially activate different synaptic mechanisms. However, Golding et al. (2002) have shown that just as bAPs can induce Hebbian LTP at CA1 pyramidal cell synapses so too can dendritically initiated action potentials. If both types of action potential are subject to Hebbian plasticity, it would make sense for both to be subject to the equalizing force of anti-STDP as well. Otherwise, one of the STDP disaster scenarios discussed here would be a likely outcome.

Previously, synaptic equalization has been referred to as distance-dependent synaptic scaling (Smith et al. 2003). In the broader context that we explore here, it seems more appropriate to refer to it as location-dependent synaptic scaling because we present it as a scaling that accounts not only for synaptic distance from the soma but also site-specific differences between dendritic regions that may not be strictly distance-dependent. Using complex, multi-compartment models to explore these issues illuminates some of the constant push-pull forces at work in real neurons, trying to maintain a stable operating regime across the entire extent of the cell and provide an opportunity for all synapses to participate in postsynaptic output without sacrificing adaptability. We believe that our simulation results make a strong case for the existence of anti-STDP as an important mechanism in this balancing process.

GRANTS

This research was supported by National Institutes of Health Grants MH-58754 and NS-47054 and by a NIH Director's Pioneer Award, part of the NIH Roadmap for Medical Research, through Grant 5-DP1-OD114-02.

REFERENCES

Abarbanel HD, Gibb L, Huerta R, and Rabinovich MI. Biophysical model of synaptic plasticity dynamics. *Biol Cybern* 89: 214–226, 2003.

Alvarez FJ, Dewey DE, Harrington DA, and Fyffe RE. Cell-type specific organization of glycine receptor clusters in the mammalian spinal cord. *J Comp Neurol* 379: 150–170, 1997.

Andersen P, Silfvenius H, Sundberg SH, and Sveen O. A comparison of distal and proximal dendritic synapses on CA1 pyramids in guinea pig hippocampal slices in vitro. *J Physiol* 307: 273–299, 1980.

Andrásfalvy BK and Magee JC. Distance-dependent increase in AMPA receptor number in the dendrites of adult hippocampal CA1 pyramidal neurons. *J Neurosci* 21: 9151–9159, 2001.

Andrásfalvy BK, Smith MA, Borchardt T, Sprengel R, and Magee JC. Impaired regulation of synaptic strength in hippocampal neurons from GluR1-deficient mice. *J Physiol* 552: 35–45, 2003.

Bell CC, Han VZ, Sugawara Y, and Grant K. Synaptic plasticity in a cerebellum-like structure depends on temporal order. *Nature* 387: 278–281, 1997.

Bi GQ and Poo MM. Synaptic modifications in cultured hippocampal neurons: dependence on spike timing, synaptic strength, and postsynaptic cell type. *J Neurosci* 18: 10464–10472, 1998.

Bi GQ and Rubin J. Timing in synaptic plasticity: from detection to integration. *Trends Neurosci* 28: 222–228, 2005.

Castellani GC, Quinlan EM, Bersani F, Cooper LN, and Shouval HZ. A model of bidirectional synaptic plasticity: from signaling network to channel conductance. *Learn Mem* 12: 423–432, 2005.

Chen X and Johnston D. Properties of single voltage-dependent K^+ channels in dendrites of CA1 pyramidal neurons of rat hippocampus. *J Physiol* 559: 187–203, 2004.

Debanne D, Gähwiler BH, and Thompson SM. Long term synaptic plasticity between pairs of individual CA3 pyramidal cells in rat hippocampal slice cultures. *J Physiol* 507: 237–247, 1998.

Dodt H-U, Frick A, Kampe K, and Zieglgänsberger W. NMDA and AMPA receptors on neocortical neurons are differentially distributed. *Eur J Neurosci* 10: 3351–3357, 1998.

Feldman DE. Timing-based LTP and LTD at vertical inputs to layer II/III pyramidal cells in rat barrel cortex. *Neuron* 27: 45–56, 2000.

Franks KM and Sejnowski TJ. Complexity of calcium signaling in synaptic spines. *Bioessays* 24: 1130–1144, 2002.

Frick A, Zieglgänsberger W, and Dodt HU. Glutamate receptors form hot spots on apical dendrites of neocortical pyramidal neurons. *J Neurophysiol* 86: 1412–1421, 2001.

Froemke RC and Dan Y. Spike-timing-dependent synaptic modification induced by natural spike trains. *Nature* 416: 433–438, 2002.

Froemke RC, Poo MM, and Dan Y. Spike-timing-dependent synaptic plasticity depends on dendritic location. *Nature* 434: 221–225, 2005.

Goldberg J, Holthoff K, and Yuste R. A problem with Hebb and local spikes. *Trends Neurosci* 25: 433–435, 2002.

Golding NL, Jung H, Mickus T, and Spruston N. Dendritic calcium spike initiation and repolarization are controlled by distinct potassium channel subtypes in CA1 pyramidal neurons. *J Neurosci* 19: 8789–8798, 1999.

Golding NL and Spruston N. Dendritic sodium spikes are variable triggers of axonal action potentials in hippocampal CA1 pyramidal neurons. *Neuron* 21: 1189–1200, 1998.

Golding NL, Staff NP, and Spruston N. Dendritic spikes as a mechanism for cooperative long-term potentiation. *Nature* 18: 326–331, 2002.

Gütig R, Aharonov R, Rotter S, and Sompolinsky H. Learning input correlations through nonlinear temporally asymmetric Hebbian plasticity. *J Neurosci* 23: 3697–3714, 2003.

Han VZ, Grant K, and Bell CC. Reversible associative depression and nonassociative potentiation at a parallel fiber synapse. *Neuron* 27: 611–622, 2000.

Häusser M. Synaptic function: dendritic democracy. *Curr Biol* 11: R10–R12, 2001.

Häusser M and Mel B. Dendrites: bug or feature? *Curr Opin Neurobiol* 13: 372–383, 2003.

Häusser M, Spruston N, and Stuart GJ. Diversity and dynamics of dendritic signaling. *Science* 290: 739–744, 2000.

Hines ML and Carnevale NT. The NEURON simulation environment. *Neural Comput* 9: 1179–1209, 1997.

Hoffman DA, Magee JC, Colbert CM, and Johnston D. K^+ channel regulation of signal propagation in dendrites of hippocampal pyramidal neurons. *Nature* 387: 869–875, 1997.

Iansek R and Redman SJ. The amplitude, time course and charge of unitary post-synaptic potentials evoked in spinal motoneuron dendrites. *J Physiol* 234: 665–688, 1973.

Jack JJB, Redman SJ, and Wong K. The components of synaptic potentials evoked in cat spinal motoneurons by impulses in single group Ia afferents. *J Physiol* 321: 65–96, 1981.

Johnston D, Magee JC, Colbert CM, and Christie BR. Active properties of neuronal dendrites. *Annu Rev Neurosci* 19: 165–186, 1996.

Kempter R, Gerstner W, and van Hemmen JL. Intrinsic stabilization of output rates by spike-based Hebbian learning. *Neural Comput* 13: 2709–2741, 2001.

Kistler WM and van Hemmen JL. Modeling synaptic plasticity in conjunction with the timing of pre- and postsynaptic action potentials. *Neural Comput* 12: 385–405, 2000.

Korn H, Bausela F, Charpier S, and Faber DS. Synaptic noise and multiquantal release at dendritic synapses. *J Neurophysiol* 70: 1249–1254, 1993.

Magee JC and Cook EP. Somatic EPSP amplitude is independent of synapse location in hippocampal pyramidal neurons. *Nat Neurosci* 3: 895–903, 2000.

Magee JC and Johnston D. Characterization of single voltage-gated Na^+ and Ca^{2+} channels in apical dendrites of rat CA1 pyramidal neurons. *J Physiol* 487: 67–90, 1995.

Mainen ZF, Joerges J, Huguenard JR, and Sejnowski TJ. A model of spike initiation in neocortical pyramidal neurons. *Neuron* 15: 1427–1439, 1995.

Markram H, Lübke J, Frotscher M, and Sakmann B. Regulation of synaptic efficacy by coincidence of postsynaptic Aps and EPSPs. *Science* 275: 213–215, 1997.

Mickus T, Jung H, and Spruston N. Properties of slow, cumulative sodium channel inactivation in rat hippocampal CA1 pyramidal neurons. *Biophys J* 76: 846–860, 1999.

Pettit DL and Augustine GJ. Distribution of functional glutamate and GABA receptors on hippocampal pyramidal cells and interneurons. *J Neurophysiol* 84: 28–38, 2000.

Pierce JP and Mendell LM. Quantitative ultrastructure of Ia boutons in the ventral horn: scaling and positional relationships. *J Neurosci* 13: 4748–4763, 1993.

Pyapali GK, Sik A, Penttonen M, Buzsaki G, and Turner DA. Dendritic properties of hippocampal CA1 pyramidal neurons in the rat: Intracellular staining in vivo and in vitro. *J Comp Neurol* 391: 335–352, 1998.

Rabinowitch I and Segev I. The interplay between homeostatic plasticity and functional dendritic compartments. *J Neurophysiol* 96: 276–283, 2006.

Roberts PD. Dynamics of temporal learning rules. *Phys Rev E* 62: 4077–4082, 2000.

Roberts PD and Bell CC. Computational consequences of temporally asymmetric learning rules. II. Sensory image cancellation. *J Comput Neurosci* 9: 67–83, 2000.

Roberts PD and Bell CC. Active control of spike-timing dependent synaptic plasticity in an electrosensory system. *J Physiol Paris* 96: 445–449, 2002.

Rubin JE. Steady states in an iterative model for multiplicative spike-timing-dependent plasticity. *Network* 12: 131–140, 2001.

Rubin JE, Gerkin RC, Bi GQ, and Chow CC. Calcium time course as a signal for spike-timing-dependent plasticity. *J Neurophysiol* 93: 2600–2613, 2005.

Rubin J, Lee DD, and Sompolinksy H. Equilibrium properties of temporally asymmetric Hebbian plasticity. *Phys Rev Lett* 86: 364–367, 2001.

Rudolph M and Destexhe A. A fast-conducting, stochastic integrative mode for neocortical neurons in vivo. *J Neurosci* 23: 2466–2476, 2003.

Rumsey CC and Abbott LF. Equalization of synaptic efficacy by activity- and timing-dependent synaptic plasticity. *J Neurophysiol* 91: 2273–2280, 2004a.

Rumsey CC and Abbott LF. Synaptic equalization by anti-STDP. *Neurocomputing* 58–60: 359–364, 2004b.

Schiller J, Schiller Y, Stuart G, and Sakmann B. Calcium action potentials restricted to distal apical dendrites of rat neocortical pyramidal neurons. *J Physiol* 505: 605–616, 1997.

Senn W, Markram H, and Tsodyks M. An algorithm for modifying neurotransmitter release probability based on pre- and postsynaptic spike timing. *Neural Comput* 13: 35–67, 2001.

Siegel M, Marder E, and Abbott LF. Activity-dependent current distributions in model neurons. *Proc Natl Acad Sci USA* 91: 11308–11312, 1994.

Sjöström PJ, Turrigiano GG, and Nelson SB. Rate, timing, and cooperativity jointly determine cortical synaptic plasticity. *Neuron* 32: 1149–1164, 2001.

Sjöström PJ, Turrigiano GG, and Nelson SB. Neocortical LTD via coincident activation of presynaptic NMDA and cannabinoid receptors. *Neuron* 39: 641–654, 2003.

Smith MA, Ellis-Davies GCR, and Magee JC. Mechanism of the distance-dependent scaling of Schaffer collateral synapses in rat CA1 pyramidal neurons. *J Physiol* 548: 245–258, 2003.

Song S and Abbott LF. Cortical development and remapping through spike-timing dependent plasticity. *Neuron* 32: 339–350, 2001.

Song S, Miller KD, and Abbott LF. Competitive Hebbian learning through spike-timing-dependent synaptic plasticity. *Nat Neurosci* 3: 919–926, 2000.

Stricker C, Field AC, and Redman SJ. Statistical analysis of amplitude fluctuations in EPSCs evoked in rat CA1 pyramidal neurons in vitro. *J Physiol* 490: 419–441, 1996.

Stuart GJ and Sakmann B. Active propagation of somatic action potentials into neocortical pyramidal cell dendrites. *Nature* 367: 69–72, 1994.

Stuart G, Schiller J, and Sakmann B. Action potential initiation and propagation in rat neocortical pyramidal neurons. *J Physiol* 505: 617–632, 1997a.

Stuart G, Spruston N, Sakmann B, and Häusser M. Action potential initiation and backpropagation in neurons of the mammalian CNS. *Trends Neurosci* 20: 125–131, 1997b.

Sur C, Triller A, and Korn H. Morphology of the release site of inhibitory synapses on the soma and dendrite of an identified neuron. *J Comp Neurol* 351: 247–260, 1995.

Turrigiano G and Nelson SB. Homeostatic plasticity in the developing nervous system. *Nat Rev Neurosci* 5: 97–107, 2004.

Triller A, Seitanidou T, Franksson O, and Korn H. Size and shape of glycine receptor clusters in a central neuron exhibit a somato-dendritic gradient. *New Biol* 2: 637–641, 1990.

Tzounopoulos T, Kim Y, Oertel D, and Trussell LO. Cell-specific, spike timing-dependent plasticities in the dorsal cochlear nucleus. *Nat Neurosci* 7: 719–725, 2004.

van Rossum MC, Bi GQ, and Turrigiano GG. Stable Hebbian learning from spike-timing-dependent plasticity. *J Neurosci* 20: 8812–8821, 2000.

Wang SS, Denk W, and Häusser M. Coincidence detection in single dendritic spines mediated by calcium release. *Nat Neurosci* 3: 1266–1273, 2000.

Williams A, Roberts PD, and Leen TK. Stability of negative-image equilibria in spike-timing-dependent plasticity. *Phys Rev E* 68: 021923, 2003.

Williams SR and Stuart GJ. Dependence of EPSP efficacy on synapse location in neocortical pyramidal neurons. *Science* 295: 1907–1910, 2002.

Williams SR and Stuart GJ. Role of dendritic synapse location in the control of action potential output. *Trends Neurosci* 26: 147–154, 2003.

Zhang LI, Tao HW, Holt CE, Harris WA, and Poo MM. A critical window for cooperation and competition among developing retinotectal synapses. *Nature* 395: 37–44, 1998.